Amino Acids (2023) 55:1023–1037
https://doi.org/10.1007/s00726-023-03292-3

ORIGINAL ARTICLE

Targeting prostate cancer with docetaxel-loaded peptide 563-conjugated PEtOx-*co*-PEI$_{30\%}$-*b*-PCL polymeric micelle nanocarriers

Ayca Ece Nezir[1] · Zeynep Busra Bolat[1,2] · Naile Ozturk[3,4] · Polen Kocak[1] · Ebru Zemheri[5] · Sevgi Gulyuz[6,7] · Umut Ugur Ozkose[6,7,8] · Ozgur Yilmaz[6] · Imran Vural[3] · Asuman Bozkır[9] · Fikrettin Sahin[1] · Dilek Telci[1]

Received: 23 June 2022 / Accepted: 5 June 2023 / Published online: 15 June 2023

Abstract

Prostate cancer is a global disease that negatively affects the quality of life. Although various strategies against prostate cancer have been developed, only a few achieved tumor-specific targeting. Therefore, a special emphasis has been placed on the treatment of cancer using nano-carrier-encapsulated chemotherapeutic agents conjugated with tumor-homing peptides. The targeting strategy coupling the drugs with nanotechnology helps to overcome the most common barriers, such as high toxicity and side effects. Prostate-specific membrane antigen has emerged as a promising target molecule for prostate cancer and shown to be targeted with high affinity by GRFLTGGTGRLLRIS peptide known as peptide 563 (P563). Here, we aimed to assess the in vitro and in vivo targeting efficiency, safety, and efficacy of P563-conjugated, docetaxel (DTX)-loaded polymeric micelle nanoparticles (P563-PEtOx-*co*-PEI$_{30\%}$-*b*-PCL-DTX) against prostate cancer. To this end, we analyzed the cytotoxic activity of P563-PEtOx-*co*-PEI$_{30\%}$-*b*-PCL and P563-PEtOx-*co*-PEI$_{30\%}$-*b*-PCL-DTX by a cell proliferation assay using PNT1A and 22Rv1 cells. We have also determined the targeting selectivity of P563-PEtOx-*co*-PEI$_{30\%}$-*b*-PCL-FITC by flow cytometry and assessed the induction of cell death by western blot and TUNEL assays for P563-PEtOx-*co*-PEI$_{30\%}$-*b*-PCL-DTX in 22Rv1 cells. To investigate the in vivo efficacy, we administered DTX in the free form or in polymeric micelle nanoparticles to athymic CD-1 nu/nu mice 22Rv1 xenograft models and performed histopathological analyses. Our study showed that targeting prostate cancer with P563-conjugated PEtOx-*co*-PEI$_{30\%}$-*b*-PCL polymeric micelles could exert a potent anti-cancer activity with low side effects.

Keywords Prostate cancer · Docetaxel · Polymeric micelle · Drug delivery · Targeted therapy · Peptide 563

Handling editor: E. Closs.

✉ Dilek Telci
dilek.telci@yeditepe.edu.tr

[1] Department of Genetics and Bioengineering, Faculty of Engineering, Yeditepe University, Inonu Mahallesi, Kayisdagi Caddesi, Atasehir, 34755 Istanbul, Turkey

[2] Department of Molecular Biology and Genetics, Faculty of Engineering and Natural Sciences, Istanbul Sabahattin Zaim University, Kucukcekmece, 34303 Istanbul, Turkey

[3] Department of Pharmaceutical Technology, Faculty of Pharmacy, Hacettepe University, Sihhiye, 06100 Ankara, Turkey

[4] Department of Pharmaceutical Technology, Faculty of Pharmacy, Inonu University, Battalgazi, 44280 Malatya, Turkey

[5] Department of Pathology, Umraniye Training and Research Hospital, University of Health Sciences, Umraniye, Istanbul, Turkey

[6] Materials Institute, Marmara Research Center, TUBITAK, Gebze, Turkey

[7] Department of Chemistry, Faculty of Science and Letters, Istanbul Technical University, Maslak, Istanbul, Turkey

[8] Department of Chemistry, Faculty of Science and Letters, Piri Reis University, Tuzla, Istanbul, Turkey

[9] Department of Pharmaceutical Technology, Faculty of Pharmacy, Ankara University, Yeni Mahalle, 06560 Ankara, Turkey

Introduction

Prostate cancer is one of the most prevalent neoplasms among men, accounting for approximately 20% of new cancer diagnoses (Salji et al. 2019). Patients with localized prostate cancer usually undergo radical surgery and radiotherapy, which can provide 10-year disease-free survival (Bill-Axelson et al. 2011; Litwin and Tan 2017). On the other hand, androgen deprivation therapy (ADT) is the first-line treatment for metastatic prostate cancer (Huggins 1942; Litwin and Tan 2017; Salji et al. 2019). However, it is unlikely to achieve complete tumor regression upon ADT, which necessitates chemotherapeutic drug administration to prevent the recurrence of the disease (Denmeade and Isaacs 2002).

Docetaxel (DTX) is an anti-neoplastic drug that belongs to the taxoid family and is one of the most commonly used agents for the treatment of several cancers, including breast, lung, ovarian, and prostate cancer (Imran et al. 2020). DTX exerts its anti-cancer effects through the stabilization of tubulin, leading to the inhibition of microtubule depolymerization and disassembly and inevitably to cycle arrest in the G_1/M phase. The potency of DTX is further increased by its ability to promote the expression of the cell cycle inhibitor p27 and inhibit the expression of the anti-apoptotic Bcl-2 gene (Tan et al. 2012). However, high lipophilicity (da Silva et al. 2018) and associated side effects of DTX, including neutropenia, hypersensitivity reactions, peripheral neuropathy, musculoskeletal toxicity, and nasolacrimal duct stenosis (Tan et al. 2012), constitute major limitations to its clinical application.

Due to the severe side effects of conventional chemotherapy, increasing attention has been paid to tumor-homing approaches (Wüstemann et al. 2018). Recent progress in nanotechnology has allowed researchers to overcome the toxicity caused by the solubilization of DTX with high concentrations of surfactants (Zhang and Zhang 2013). Numerous lipid-, polymer-, and albumin-based nanocarrier formulations have been developed for the delivery of anti-cancer agents with enhanced tumor accumulation, reduced systemic toxicity, and improved therapeutic efficacy (Narvekar et al. 2014). For example, DTX-loaded PAMAM-based poly (γ-benzyl-L-glutamate)-b-D-α tocopherol polyethylene glycol 1000 succinate nanoparticles (NPs) (Wang et al. 2019), DTX-loaded trastuzumab-coated lipid polymer NPs (Zhang et al. 2019), DTX-loaded poloxamer (PLX-188)-coated poly (lactic-co-glycolic acid) NPs (Chishti et al. 2019), chitosan and sodium tripolyphosphate-based ionically cross-linked NPs (Mahmood et al. 2019), and DTX-loaded poly (ethylene glycol) functionalized gold nanoparticles (Thambiraj et al. 2021) have shown an improvement in controlled release and higher cancer cell toxicity compared with free DTX administration. Moreover, accumulating evidence suggests that polymeric drug carriers are the most effective functionalized carriers due to the versatility of their use and chemical modification (Mandracchia et al. 2014; Tripodo et al. 2013).

Polymeric micelles are NPs formed by the spontaneous self-assembly of amphiphilic polymers, hence consisting of a hydrophobic core and hydrophilic shell. Their small size ranging between 50 and 100 nm allows their extravasation into tumors through enhanced permeability and retention (EPR) effect that relies on the (i) hyper-vascularity and incomplete vascular architecture of solid tumors, (ii) secretion of vascular permeability factors stimulating extravasation within a cancer tissue, and (iii) the absence of effective lymphatic drainage from tumors impeding the efficient clearance of macromolecules accumulated in the solid tumor tissues (Matsumura and Kataoka 2009). Moreover, the lipidic core of polymeric micelles is suitable for holding lipophilic drugs such as DTX, and their high thermodynamic stability prevents premature drug release. Currently, numerous polymeric micelles are in clinical trials (Varela-Moreira et al. 2017), including several DTX-loaded formulations (Alven and Aderibigbe 2020).

In addition to the EPR effect, the tumor selectivity of NPs can be improved by the utilization of active targeting (Wüstemann et al. 2018). One of the most common approaches is the encapsulation of drugs in a suitable carrier conjugated with specific tumor-targeting agents, such as antibodies, vitamins, hormones, and peptides, with the ability to selectively target the tumor and its microenvironment (Tripodo et al. 2014). Prostate-specific membrane antigen (PSMA) is a membrane-bound protease that is usually overexpressed in malignant prostate cancer cells (Carter et al. 1996; Wüstemann et al. 2018). PSMA has been considered an attractive target molecule due to its association with the aggressive disease state (Gao et al. 2015; Kiess et al. 2015; Barrio et al. 2016; Haberkorn et al. 2016). Our group and others identified peptide 563 (GRFLTGGTGRLLRIS) as an important high-affinity tumor-homing peptide for PSMA (Shen et al. 2013; Nezir et al. 2021). Peptide 563 (P563) offers the advantage of small size, excellent tissue penetration, easy chemical incorporation into drugs, and low immunogenicity.

In this study, in vitro and in vivo anti-tumor efficacy of a novel DTX-loaded P563-conjugated poly(2-ethyl-2-oxazoline)-*co*-polyethylenimine-*block*-poly(ε-caprolactone) (P563-PEtOx-*co*-$PEI_{30\%}$-*b*-PCL-DTX) polymeric micelle formulation was evaluated using PSMA-positive 22Rv1 prostate cancer cells.

Materials and methods

Preparation of P563-PEtOx-*co*-PEI$_{30\%}$-*b*-PCL polymeric micelles

Synthesis and characterization of PEtOx-*co*-PEI-*b*-PCL amphiphilic block copolymers were reported previously (Gulyuz et al. 2018; Kara et al. 2018; Ozturk et al. 2020). Conjugation of P563 (GRFLTGG TGRLLRIS) with PEtOx-*co*-PEI-*b*-PCL copolymer was described in an earlier study (Gulyuz et al. 2021). PEtOx$_{7500(\%70)}$-*co*-PEI$_{1400(\%30)}$-*b*-PCL$_{2100}$ block copolymer and P-563 conjugated PEtOx$_{7500(\%70)}$-*co*-PEI$_{1400(\%30)}$-*b*-PCL$_{2100}$ block copolymer were used at a ratio of 4:1 to prepare P563-PEtOx-*co*-PEI$_{30\%}$-*b*-PCL micelles. The polymer:drug ratio of DTX-loaded (Doxitax, Kocak Farma Ltd, Turkey) micelles (P563-PEtOx-*co*-PEI$_{30\%}$-*b*-PCL-DTX) was 10:1 (mg/mg). DTX and polymer were dissolved in methanol (4 mL), and then methanol was evaporated by a rotary evaporator. The obtained thin film was hydrated by adding ultra-pure water (60 °C) and agitation with vortex for 5 min. Next, the micelles were centrifuged at 9500 x*g* for 3 min to precipitate free DTX and large aggregates.

Sodium fluorescein-loaded (P563-PEtOx-co-PEI30%-b-PCL-FITC) micelles were prepared by the same method used to prepare DTX-loaded micelles, with slight modification. Sodium fluorescein and the polymer were dissolved in methanol (4 mL), and then methanol was evaporated by a rotary evaporator. The resulting thin film was hydrated by the addition of ultra-pure water (60ºC) and agitation with vortex for 5 min. The obtained micelle suspension was filtered using a 0.22 µm filter and then centrifuged at 4146 x*g* (for 20 min) using Amicon centrifugal filters (MWCO 3000 Da) to separate free sodium fluorescein.

Characterization of P563-PEtOx-*co*-PEI$_{30\%}$-*b*-PCL polymeric micelles

Particle size, polydispersity index (PDI), and zeta potential (ZP) of micelles were determined using a Zetasizer (Nano-ZS, Malvern Instruments Ltd., UK). All measurements were performed in triplicate. The micelle formulation was lyophilized for 48 h using a freeze-dryer (Labconco, USA) to determine the encapsulated DTX amount. The freeze-dried micelle powder was dissolved in methanol, and the DTX amount was analyzed by an HPLC method where a 45:55 (v/v) mixture of water and acetonitrile was used as the mobile phase. The chromatographic column was a reverse-phase C18 column (250 mm × 4.6 mm, pore size 5 µm, Inertsil ODS-3, USA), and the detection wavelength was 227 nm. Encapsulation efficiency (EE) was calculated according to the following equation:

$$EE = (\text{amount of DTX loaded to micelles}) / (\text{initial amount of DTX}) \times 100$$

DTX release from micelles was determined in phosphate buffer (pH 7.4) using dialysis cassettes (MWCO 3500 Da) at 37 °C for 72 h. Dialysis cassettes filled with 0.75 mL of the formulation were placed in the constantly stirred dialysis medium (2 L of phosphate buffer, pH 7.4). Samples were then withdrawn from the dialysis cassettes to determine residual drug amounts at predetermined time points. These samples were analyzed by HPLC at 227 nm to calculate the released drug amount.

The amount of sodium fluorescein loaded into P563-PEtOx-co-PEI30%-b-PCL-FITC micelles was determined indirectly by the analysis of the filtrate obtained after centrifugation with Amicon tubes using a spectrofluorometer (excitation wavelength: 485 nm, emission wavelength: 515 nm).

For morphological analysis, the micelle formulation was dropped (10 µL) onto a carbon grid with a micropipette and air-dried. Next, the sample was analyzed with transmission electron microscopy (TEM) (Tecnai G2 Spirit BioTwin, FEI Company, Fremont, CA) to visualize the micelle morphology.

Serum stability studies of the peptide-targeted DTX-loaded micelle formulations (P563-PEtOx-*co*-PEI$_{30\%}$-*b*-PCL-DTX) were performed in PBS solution supplemented with serum component as 10% FBS. The micelle formulations were incubated at 37 °C, and the particle size (nm), ZP (mV), and PDI of the formulations were determined at specified time intervals.

Cell culture

PNT1A human prostate epithelial cells (95,012,614) were obtained from Sigma Aldrich, USA. 22Rv1 human prostate carcinoma cells (CRL-2505) were obtained from American Type Culture Collection (ATCC®). The cells were maintained in Roswell Park Memorial Institute (RPMI) 1640 medium (Gibco™ Thermo Fisher Scientific, USA) supplemented with 10% (v/v) fetal bovine serum (FBS; Gibco™) and 100 units/mL penicillin/streptomycin (Gibco™) in a humidified incubator at 37 °C and 5% CO_2.

Assessment of cell viability

Cytotoxicity of PEtOx-*co*-PEI$_{30\%}$-*b*-PCL block copolymer on PNT1A normal prostate epithelial cells was assessed by WST-1 cell proliferation assay (Roche, USA). Briefly,

5×10^4 cells were seeded into 96-well plates. After cell attachment, the cells were treated with 0, 100, 200, 300, 400, or 500 µg/mL of PEtOx-*co*-$PEI_{30\%}$-*b*-PCL block copolymer sub-stocks for 24–96 h. The cells were subjected to WST-1 reagent at every 24 h interval, as per the manufacturer's instructions, and absorbance values were measured at 450 nm wavelength, using SpectraMax Paradigm Multi-Mode Microplate Reader (Molecular Devices, San Jose, CA, USA). PEtOx-*co*-$PEI_{30\%}$-*b*-PCL-DTX micelle toxicity on 22Rv1 prostate cancer cells was evaluated following the same procedure, for 0, 0.01, 0.05, 0.1, 0.25, and 0.50 µg/mL of DTX. Empty micelle (PEtOx-*co*-$PEI_{30\%}$-*b*-PCL) was diluted to obtain equal amounts of polymer/mL as the respective PEtOx-*co*-$PEI_{30\%}$-*b*-PCL-DTX sub-stocks.

Flow cytometry

In order to determine the prostate cancer-targeting efficiency, micelle formulations loaded with fluorescein (P563-PEtOx-*co*-$PEI_{30\%}$-*b*-PCL-FITC) were prepared. PNT1A and 22Rv1 cells were seeded into 6-well plates at a density of 3×10^5 cells/well. The cells were allowed to attach overnight and then subjected to 0.5 mg/mL of P563-PEtOx-*co*-$PEI_{30\%}$-*b*-PCL-FITC for 30 min at 37 °C. After extensive washing with PBS, the cells were scraped and fixed with 0.05% (w/v) formaldehyde. FITC-positive cells were counted using the FL-1 channel of the Becton Dickinson FACSCalibur™ flow cytometer. Untreated cells were utilized as the negative control to set the parameters of the forward and side scatter. Histogram plots were generated using CellQuestPro software, where the percentages of FITC-positivity within the whole cell populations were calculated (Becton Dickinson, USA).

Detection of apoptotic cell death

Total protein was isolated from 22Rv1 cells treated with PEtOx-*co*-$PEI_{30\%}$-*b*-PCL-DTX micelles carrying 0.05 µg/mL of DTX for 48 h. PEtOx-*co*-$PEI_{30\%}$-*b*-PCL micelle was diluted to obtain an equal amount of polymer/mL as the respective PEtOx-*co*-$PEI_{30\%}$-*b*-PCL-DTX sub-stock. Untreated cells were utilized as the negative control. Briefly, cells collected in RIPA buffer were separated on 12% SDS-PAGE gels and blotted for Pan-Actin (Cell Signaling Technology [CST], MA, USA; 8456), cleaved caspase-9 (CST 9502), cleaved caspase-3 (CST 9661), and cleaved PARP (CST 5625) primary antibodies produced in rabbit. Following secondary antibody incubation, the HRP signal was developed with an enhanced chemiluminescence solution, and the protein bands were detected using ChemiDoc XRS+ (BioRad, USA).

Apoptotic cells were also detected using in Situ Cell Death Detection Kit (Roche, USA), following the manufacturer's instructions. Briefly, 1.2×10^7 22Rv1 cells in 6-well plates were treated with PEtOx-*co*-$PEI_{30\%}$-*b*-PCL-DTX containing 0.05 µg/mL of DTX or an equal amount of PEtOx-*co*-$PEI_{30\%}$-*b*-PCL in complete medium for 48 h. Untreated cells were used as the negative control. The cells were collected and fixed with 4% (w/v) paraformaldehyde solution on a thermal shaker at 37 °C for 1 h. The cells were permeabilized with 0.1% (v/v) Triton X-100 (MP Biomedical, France) in 0.1% (w/v) sodium citrate solution for 2 min on ice. After washing with 1X PBS, labeling was performed by incubating the cells in the TUNEL reaction mixture (containing Label Solution and Enzyme Mix) on a thermal shaker at 37 °C for 75 min. Finally, the cells were washed twice with PBS, and the cell populations were analyzed by flow cytometry, as described in "Flow Cytometry".

Determination of in vivo anti-tumor activity

For in vivo anticancer studies, athymic male CD-1 nu/nu mice (5–6 weeks of age, 20 ± 2 g) obtained from Charles River Laboratories (Germany) were maintained in the animal facility of Yeditepe University (Turkey) in accordance with and approved by Animal Care and Welfare Committee of Yeditepe University (Turkey, decision #644). The animals had access to food and water ad libitum. We have optimized a matrigel-based orthotopic tumor inoculation method using 12×10^6 cells/100 µL for tumor inoculation at a 2:1 (v/v) ratio with BD Matrigel™ Basement Membrane Matrix (BD Biosciences, Franklin Lakes, NJ, USA). Following the third day of inoculation, mice were injected intraperitoneally (i.p.) once every three days with vehicle control, PEtOx-*co*-$PEI_{30\%}$-*b*-PCL polymeric micelle, PEtOx-*co*-$PEI_{30\%}$-*b*-PCL-DTX (2 mg/kg DTX), or free DTX (2 mg/kg) for a total of 8 injections. Tumor size and weight of each animal were measured before every injection, and mice were examined for morbidity and mortality until the end of the study. After 24 days of treatment, mice were sacrificed by cervical dislocation, and tumor volumes (mm^3) were calculated after the resection of tumors by the following formula: "Tumor volume $= 1/2(\text{Length} \times (\text{Width})^2)$" (Zhao et al. 2022), where, "Length" is the long radius and "Width" is the short radius.

Histopathological analysis

For the preparation of formalin-fixed paraffin-embedded (FFPE) samples, heart, liver, spleen, lung, and kidney were isolated and fixed at 10% formalin and processed in the Department of Pathology at Umraniye Training and Research Hospital. Paraffin sections were processed for hematoxylin and eosin (H&E) staining and evaluated by a specialized pathologist (Nayman et al. 2019). Tumor tissue samples were assessed in terms of necrosis, inflammation,

and fibrosis. Each assessment was scored between 0 and 3 (0, absent; 1, mild; 2, moderate; and 3, severe).

Statistical analysis

All data were expressed as mean ± standard deviation (SD). Differences between groups were assessed using a two-tailed Student's *t* test or ANOVA followed by a Tukey post hoc test using GraphPad Prism 8 (GraphPad Software, USA). The results were considered statistically significant at $P \leq 0.05$ (*), $P \leq 0.01$ (**), $P \leq 0.001$ (***), and $P \leq 0.0001$ (****).

Results

Effect of PEtOx-*co*-PEI$_{30\%}$-*b*-PCL polymeric micelles on cell proliferation

PEtOx-*co*-PEI$_{30\%}$-*b*-PCL block copolymers and polymeric micelles were synthesized and characterized previously (Kara et al. 2018). The safety profile of PEtOx-*co*-PEI$_{30\%}$-*b*-PCL block copolymer was reported in a previous study of our group (Gulyuz et al. 2021) by demonstrating its effects on human dermal fibroblast (HDF), human kidney cell line (HEK293), prostate epithelial cell line (PNT1A), and mesenchymal stem cells (MSC) cell proliferation. In this study, WST-1 cell proliferation assay was performed in order to determine the potential cytotoxic effects of PEtOx-*co*-PEI$_{30\%}$-*b*-PCL micelles on HDF, human hepatoblastoma (Hep-G2), PNT1A, and human fetal osteoblast (hFOB 1.19) cell proliferation. The cells were treated with PEtOx-*co*-PEI$_{30\%}$-*b*-PCL micelles at a concentration range of 100–500 µg/ml from 24 to 96 h. None of the tested doses induced a significant change in the cell proliferation rate of the human cell lines at 24 or 48 h (Fig. 1). However, a significant 40% reduction in the viability of HDF cells in comparison to the untreated cells was observed at the end of 72 h upon treatment with 400 and 500 µg/ml of the PEtOx-*co*-PEI$_{30\%}$-*b*-PCL micelle (Fig. 1a). Moreover, the reduction in HDF cell viability was dropped down to 50% upon treatment with 500 µg/mL of the PEtOx-*co*-PEI$_{30\%}$-*b*-PCL micelle at the end of 96 h. However, no such inhibitory effect on cell proliferation was observed for Hep-G2 or hFOB 1.19 cell lines (Fig. 1b and c).

Next, we evaluated the effects of PEtOx-*co*-PEI$_{30\%}$-*b*-PCL micelles on human prostate epithelial (PNT1A) cells. Approximately 20–30% and 10–20% increases in cell proliferation were observed for the tested doses at 24 and 48 h, respectively (Fig. 1d). A non-significant 10% decrease in PNT1A cell viability was observed upon treatment with

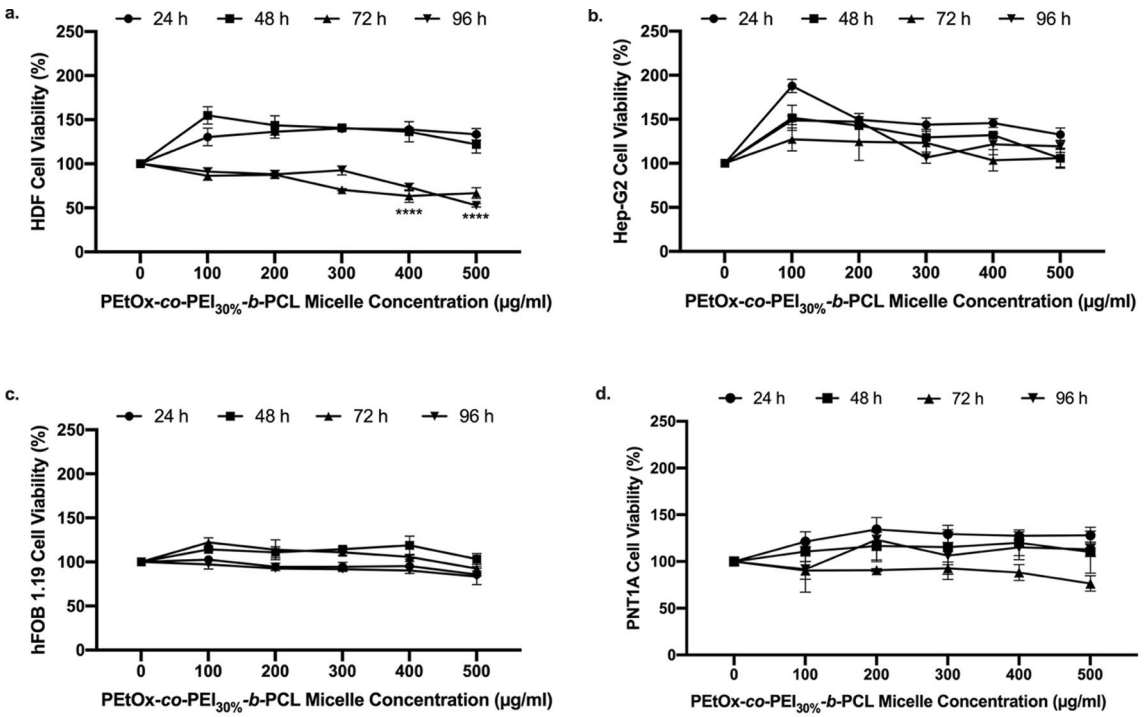

Fig. 1 Effects of PEtOx-*co*-PEI$_{30\%}$-*b*-PCL micelles on **a** HDF, **b** Hep-G2, **c** hFOB 1.19, and **d** PNT1A cell viability. Cells were treated with 0–500 µg/mL of PEtOx-*co*-PEI$_{30\%}$-*b*-PCL polymeric micelles for 24–96 h. Cell viability was assessed at the end of each 24 h interval. The viability of non-treated cells (0 µg/mL) was set as 100% to determine the relative cell viability for each condition ($n = 3$). The bars represent mean ± SD. Significant reductions in cell viability at 96 h with respect to untreated cells are shown. ****$P \leq 0.001$

100–400 µg/mL of PEtOx-*co*-$PEI_{30\%}$-*b*-PCL micelles at 72 h. For 500 µg/mL of the micelles, the decrease in cell viability was about 15% ($P > 0.05$). At the end of 96 h, there was no significant change in the viability of PNT1A cells treated with PEtOx-*co*-$PEI_{30\%}$-*b*-PCL micelles up to 500 µg/mL concentration (Fig. 1d). Collectively, these results implicated that PEtOx-*co*-$PEI_{30\%}$-*b*-PCL polymeric micelles showed no cytotoxic effect on normal prostate epithelial cells.

Characteristics of P563-PEtOx-*co*-$PEI_{30\%}$-*b*-PCL-DTX polymeric micelles

Micelle size distribution was analyzed by dynamic light scattering. The size, PDI, ZP, and encapsulation efficiency of the micelle formulations are given in Table 1. For the tumor-targeted delivery, a size range of 10–200 nm was suggested (Yokoyama 2014). The particle sizes of blank micelles and DTX-loaded micelles were around 146 nm (PDI: 0.2) and 236 nm (PDI: 0.5), respectively, indicating that drug loading increased the micelle size and PDI. Despite this increase, the micelle size still remained in a range that is considered to be suitable for tumor-targeting. PDI values can range between 0.0 and 1.0, and values < 0.05 are generally indicative of monodisperse samples, whereas values > 0.7 are seen in polydisperse systems (Mudalige et al. 2019). In drug delivery applications of polymeric/lipid-based carriers, PDI values < 0.3 are considered acceptable; however, there are no PDI criteria set by the regulatory authorities yet (Danaei et al. 2018). PDI values below 0.5 are indicative of a homogenous narrow size distribution, which applies to our results (Mudalige et al. 2019). ZP provides information on electrostatic repulsive forces, which is one of the factors that affect the colloidal stability of nano-carriers, such as van der Waals forces and steric interactions. ZP values of ± 20–30 mV and > ± 30 mV are considered relatively stable and highly stable, respectively (Bhattacharjee 2016). Our results for ZP values (19.6 ± 0.8–26.1 ± 0.9 mV) indicate the stability of the micelle formulations. DTX encapsulation was around 30% for the polymer:drug feeding ratio of 10:1. In addition to DTX-loaded micelles, FITC-loaded micelles were prepared to determine prostate cancer-targeting efficiency of P563-conjugated micelles. Size, PDI, and ZP values of P563-PEtOx-*co*-$PEI_{30\%}$-*b*-PCL-FITC were similar/close to P563-PEtOx-*co*-$PEI_{30\%}$-*b*-PCL-DTX micelles; therefore, found to be suitable for studying the targeting efficiency of peptide-conjugated micelles.

Drug release from micelles was monitored for 72 h in vitro. The release profile for DTX in pH 7.4 phosphate buffer was given in Fig. 2. During the initial 3 h, 32% of DTX was released, while 60%, 91%, and 95% DTX release were achieved at 24, 48, and 72 h, respectively. The rapid DTX release during the first 3 h could be due to the adsorbed DTX amount on micelles. The gradual increase in the released DTX amount following the first 3 h is indicative of a controlled drug release. In the case of targeted micelles, drug release from micelles should be neither too fast nor too slow. In case of abrupt drug release, the released drug in systemic circulation loses its targeting ability. On the contrary, in case of inadequately-slow drug release, efficient pharmacological action cannot be achieved in spite of successful targeting (Yokoyama 2014). P563-PEtOx-*co*-PEI30%-*b*-PCL-DTX micelles were able to achieve a sustained release for the entrapped DTX.

TEM analysis was performed to visualize polymeric micelle morphology. TEM micrographs of empty (PEtOx-*co*-$PEI_{30\%}$-*b*-PCL) and DTX-loaded P563-conjugated micelles (P563-PEtOx-*co*-$PEI_{30\%}$-*b*-PCL-DTX) were given in Fig. 3. Both empty and DTX-loaded micelles had spherical-like morphology. Empty micelles were

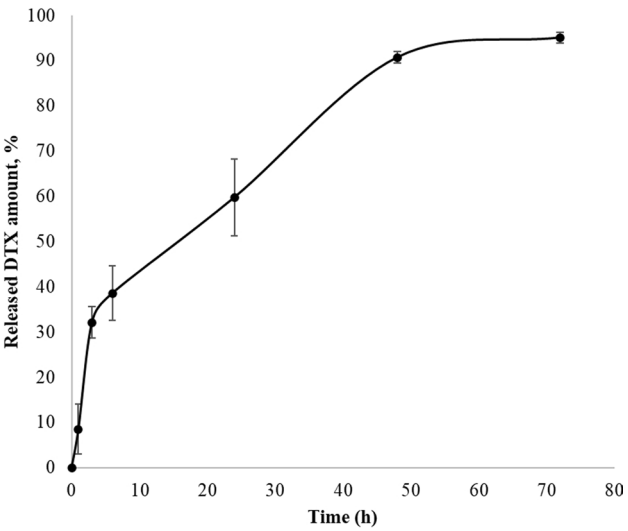

Fig. 2 DTX release from P563-conjugated micelles (P563-PEtOx-co-PEI30%-b-PCL-DTX) in pH 7.4 phosphate buffer

Table 1 Size, polydispersity index, zeta potential, and encapsulation efficiency of the micelle formulations

Micelle	Size (nm)	PDI	ZP (mV)	EE (%)
P563-PEtOx-*co*-$PEI_{30\%}$-*b*-PCL	145.9 ± 1.6	0.2 ± 0.0	19.6 ± 0.8	–
P563-PEtOx-*co*-$PEI_{30\%}$-*b*-PCL-DTX	235.6 ± 8.7	0.5 ± 0.0	26.1 ± 0.9	30.2 ± 6.9
P563-PEtOx-*co*-$PEI_{30\%}$-*b*-PCL-FITC	311.6 ± 9.9	0.3 ± 0.0	23.4 ± 1.7	94.3 ± 0.1

EE encapsulation efficiency, *PDI* polydispersity index, *ZP* zeta potential

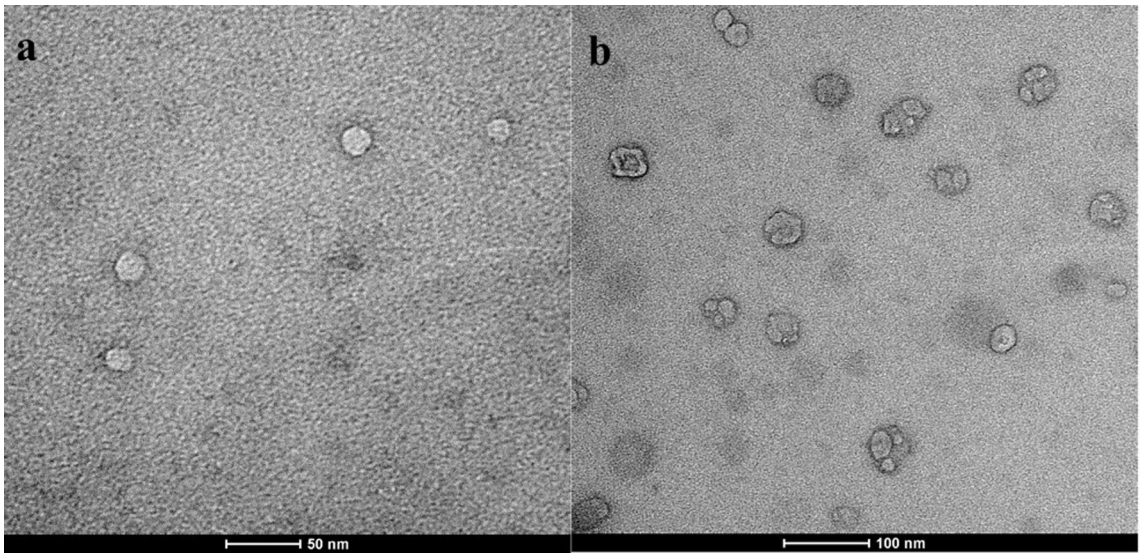

Fig. 3 TEM images of **a** PEtOx-co-PEI30%-b-PCL and **b** P563-PEtOx-co-PEI30%-b-PCL-DTX micelles

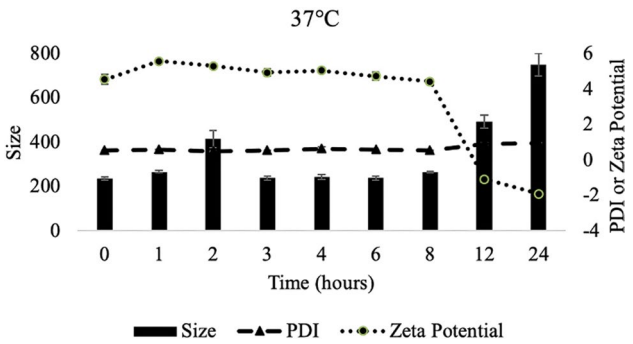

Fig. 4 Serum stability results of DTX-loaded polymeric micelles, constructed by P563- PEtOx-*co*-$PEI_{30\%}$-*b*-PCL ($n = 3$). The formulation was incubated in 10% serum at 37 °C for 24 h, and particle size, PDI, and ZP were measured at indicated time points

visualized as separate individual micelles, while DTX-loaded micelles were aggregated to some extent. The small and slightly larger micelles seen in Fig. 3b confirmed the dynamic light scattering results that indicated an increase in micelle size and polydispersity upon DTX loading.

The serum stabilities of PEtOx-*co*-$PEI_{30\%}$-*b*-PCL-DTX micelles were tested by measuring the particle size, ZP, and PDI. No significant change was observed in the mean particle size of the polymeric micelles after 8 h in 10% FBS at 37 °C (Fig. 4). At the end of 12 h, the particle size increased from 238 to 494 nm, while an increase to 753 nm in the particle size was detected after 24 h. The 4-mV ZP of the micelles declined to − 2 mV after the 24 h serum incubation. A non-significant increase in PDI was observed at the end of 24 h, indicating maintenance of the integrity of the formulations in serum.

Specificity of PEtOx-*co*-$PEI_{30\%}$-*b*-PCL micelles

Previously, we showed that p563 specifically targets 22Rv1 cells over normal PNT1A cells (Nezir et al. 2021). In order to show the targeting efficiency of PEtOx-*co*-$PEI_{30\%}$-*b*-PCL micelles, FITC-encapsulated constructs were used to treat PNT1A and 22Rv1, and FITC-positive cells were then analyzed. Flow cytometry analysis revealed that P563-PEtOx-*co*-$PEI_{30\%}$-*b*-PCL-FITC polymeric micelles showed significantly higher uptake by PSMA-positive 22Rv1 prostate cancer cells (34.43 ± 3.41%) compared with PNT1A normal prostate epithelial cells (17.50 ± 5.34%), accounting for about 2-folds (Fig. 5a). Representative histograms are shown in Fig. 5b. The results demonstrated that the cargo molecules could be selectively delivered to prostate cancer cells by P563-PEtOx-*co*-$PEI_{30\%}$-*b*-PCL micelle formulations.

Effect of DTX delivered by P563-PEtOx-*co*-$PEI_{30\%}$-*b*-PCL micelles on prostate cancer cell proliferation

The cytotoxic effect of P563-PEtOx-*co*-$PEI_{30\%}$-*b*-PCL-DTX micelles on 22Rv1 cells was analyzed using WST-1 cell proliferation assay. 22Rv1 cells were subjected to increasing concentrations of either P563-PEtOx-*co*-$PEI_{30\%}$-*b*-PCL-DTX or free DTX for 24–72 h (Fig. 6). Equal amounts of empty carriers (P563-PEtOx-*co*-$PEI_{30\%}$-*b*-PCL) corresponding to each dose were also tested. At 24 h, both P563-PEtOx-*co*-$PEI_{30\%}$-*b*-PCL-DTX and free DTX at a concentration of

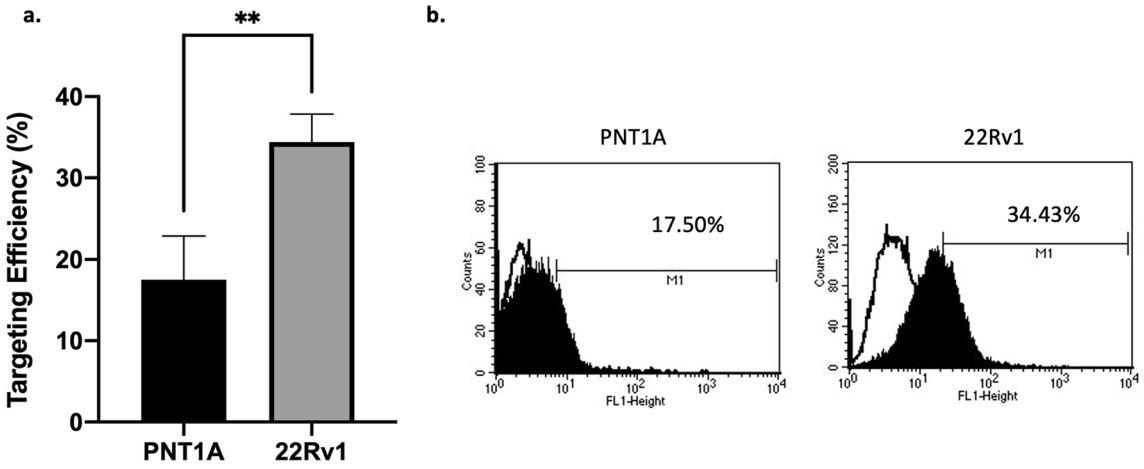

Fig. 5 Targeting efficiency of P563-PEtOx-*co*-$PEI_{30\%}$-*b*-PCL-FITC by flow cytometry. Cells were treated with 50 µg/ml of P563-PEtOx-*co*-$PEI_{30\%}$-*b*-PCL-FITC at 37 °C for 30 min. Untreated cells were used as the control group to discriminate FITC-positive cells, which were detected as the percentage of the gated total cell population. The percentage of the FITC-positive cells was measured in the FL1 channel, as indicated on the histogram graphs. The histograms are representatives of 3 independent experiments. Data are expressed as mean ± SD. $^{**}P \leq 0.01$

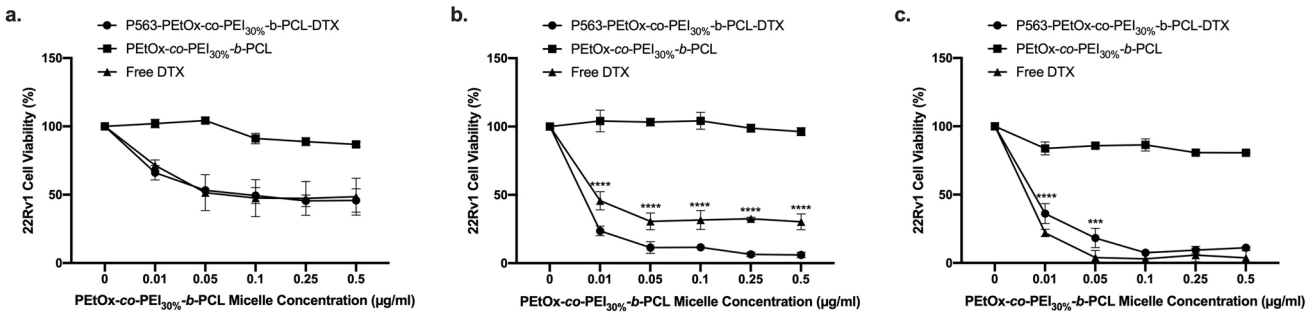

Fig. 6 Determination of the cytotoxicity of P563-PEtOx-*co*-$PEI_{30\%}$-*b*-PCL-DTX and free DTX on 22Rv1 cells. The cells were treated with 0.01–0.5 µg/ml of DTX in the carrier and in free form for **a** 24, **b** 48, and **c** 72 h. At each 24 h interval, cell viability was assessed by measuring the absorbance values at 450 nm. Data represent the average of three independent experiments ± SD. Significant differences between the viabilities of PEtOx-*co*-$PEI_{30\%}$-*b*-PCL-DTX- and free DTX-treated cells are shown. $^{***}P \leq 0.001$, $^{****}P \leq 0.0001$

0.01 µg/mL resulted in about 35% decrease in 22Rv1 cell viability, whereas treatment with P563-PEtOx-*co*-$PEI_{30\%}$-*b*-PCL-DTX and free DTX from 0.05 to 0.5 µg/mL resulted in about 50% decrease in cell viability (Fig. 6a). PEtOx-*co*-$PEI_{30\%}$-*b*-PCL carrier at indicated concentrations did not induce a significant change in cell proliferation at the time points tested (Fig. 6a–c). At 48 h, a significant 80 to 95% decrease was observed in the viability of P563-PEtOx-*co*-$PEI_{30\%}$-*b*-PCL-DTX-treated cells in a dose-dependent manner (Fig. 6b). Free DTX also reduced the viability of 22Rv1 cells, albeit with less potency, by 60% at 0.01 µg/mL and about 70% at 0.05–0.5 µg/ml. At this time point, P563-PEtOx-*co*-$PEI_{30\%}$-*b*-PCL-DTX caused a significantly higher reduction in cell proliferation than the corresponding doses of free DTX ($P < 0.001$). A significant difference in cellular responses to P563-PEtOx-*co*-$PEI_{30\%}$-*b*-PCL-DTX (35% and 15% viability) and free DTX (20% and 5% viability) were also evident for 0.01 and 0.05 µg/mL of DTX, respectively, at 72 h (Fig. 6c). At higher doses, both treatments resulted in a significant 90–95% decrease in 22Rv1 cell viability, albeit with no significant difference between the effects of P563-PEtOx-*co*-$PEI_{30\%}$-*b*-PCL-DTX and free DTX (Fig. 6c).

Collectively, these data indicate that the peptide-conjugated empty carrier did not cause toxicity, and P563-PEtOx-*co*-$PEI_{30\%}$-*b*-PCL-DTX and free DTX exerted comparable toxicity on 22Rv1 prostate cancer cells, except for 48 h, where P563-PEtOx-*co*-$PEI_{30\%}$-*b*-PCL-DTX caused a significant 30% higher decrease in viability.

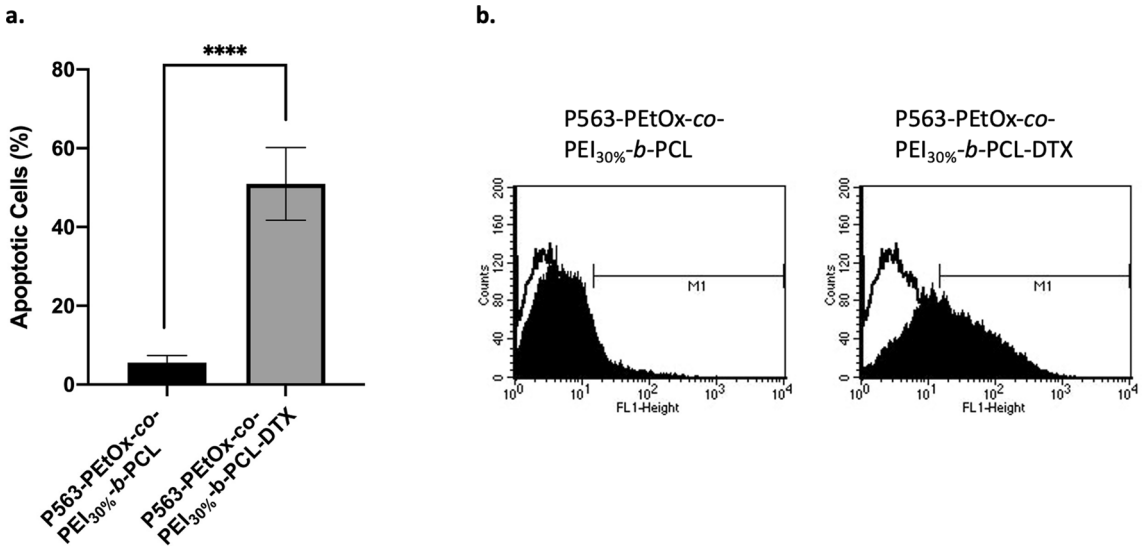

Fig. 7 Cell death induced by PEtOx-*co*-PEI$_{30\%}$-*b*-PCL-DTX micelles. **a** Percentage of apoptotic cells detected by TUNEL assay. The bars represent mean ± SD ($n = 3$); ****$P \leq 0.0001$. **b** Representative histograms showing the FITC-positive apoptotic cells detected by flow cytometry

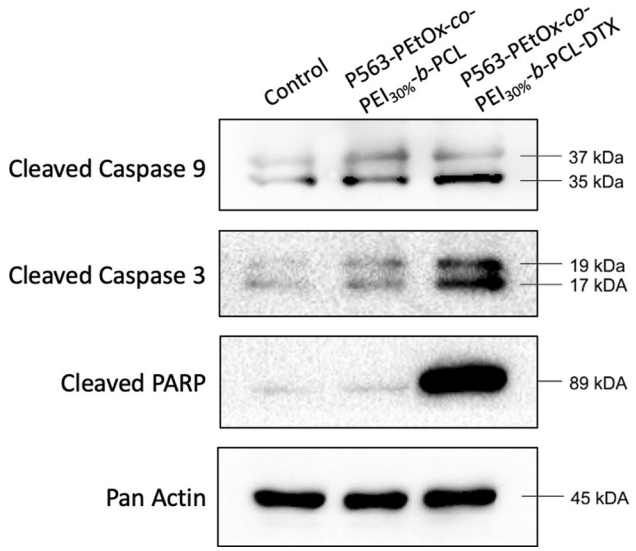

Fig. 8 Evaluation of apoptosis in 22Rv1 cells induced by 48 h treatment with PEtOx-*co*-PEI$_{30\%}$-*b*-PCL and PEtOx-*co*-PEI$_{30\%}$-*b*-PCL-DTX (0.05 µg/ml) polymeric micelles by western blotting. Protein samples were blotted against the apoptotic markers cleaved caspase-9, cleaved caspase-3, and cleaved PARP. The blots are representative of three independent experiments

Determination of cell death induced by P563-PEtOx-*co*-PEI$_{30\%}$-*b*-PCL-DTX micelles

Based on the cell viability results, 48 h incubation was selected to analyze cell death in 22Rv1 cells subjected to PEtOx-*co*-PEI$_{30\%}$-*b*-PCL or PEtOx-*co*-PEI$_{30\%}$-*b*-PCL-DTX (0.05 µg/ml DTX) by TUNEL (Fig. 7) and western blotting (Fig. 8). A significant 40% apoptotic cell death was detected upon treatment with PEtOx-*co*-PEI$_{30\%}$-*b*-PCL-DTX, while the apoptotic cell population was as low as 5% in 22Rv1 cells treated with the empty carrier.

Cell death was also analyzed by detection of caspase-9/3 and PARP cleavage using western blotting under the same experimental conditions. Both caspase-9, caspase-3, and PARP cleavage were apparent upon treatment with PEtOx-*co*-PEI$_{30\%}$-*b*-PCL-DTX, compared with the untreated control and PEtOx-*co*-PEI$_{30\%}$-*b*-PCL treated cells (Fig. 8).

Therapeutic efficacy of P563-PEtOx-*co*-PEI$_{30\%}$-*b*-PCL-DTX on prostate cancer xenograft models

Prostate cancer xenograft models were established by subcutaneous injection of 22Rv1 cells into the right flanks of CD1 nu/nu male mice to investigate the antitumor efficacy of P563- PEtOx-*co*-PEI$_{30\%}$-*b*-PCL-DTX polymeric micelles in vivo. The mice were treated with the vehicle control (PBS), P563-PEtOx-*co*-PEI$_{30\%}$-*b*-PCL, P563-PEtOx-*co*-PEI$_{30\%}$-*b*-PCL-DTX, or free DTX (2 mg/kg/3d). The average body weight of mice did not differ significantly between the vehicle and drug groups (Fig. 9). However, P563-PEtOx-*co*-PEI$_{30\%}$-*b*-PCL treatment resulted in a significant 10 g weight gain at the end of 28 d.

Tumor volume and tumor weight between mice treated with P563-PEtOx-*co*-PEI$_{30\%}$-*b*-PCL (empty carrier) showed an average tumor volume of 1420 mm^3 (Fig. 10a) and an average tumor weight of 960 mg (Fig. 10b), while the vehicle control-treated group showed tumor growth with 510 mm^3 and 543 mg, suggesting that administration of the empty carrier had a tumor growth-promoting effect. Compared with

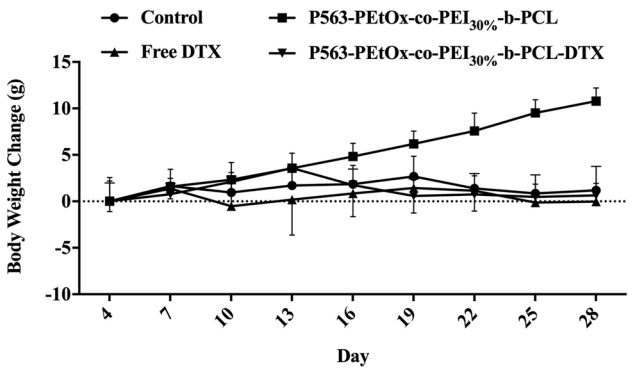

Fig. 9 Changes in body weight of CD-1 nu/nu male mice ($n=5$) upon treatment with the vehicle control, P563-PEtOx-*co*-PEI$_{30\%}$-*b*-PCL, free DTX, or P563-PEtOx-*co*-PEI$_{30\%}$-*b*-PCL -DTX. *$P \leq 0.05$, **$P \leq 0.01$

the P563-PEtOx-*co*-PEI$_{30\%}$-*b*-PCL (empty carrier) group, a significant reduction in tumor volume was achieved in the P563-PEtOx-*co*-PEI$_{30\%}$-*b*-PCL-DTX (50%) and free DTX (42%) groups. The average reduction in tumor volume between the free DTX and P563-PEtOx-*co*-PEI$_{30\%}$-*b*-PCL-DTX groups was not statistically significant ($P=0.09$). Tumor weight was reduced to 43% (415 mg) upon administration of free DTX, while a significant reduction down to 27% (254 mg) was observed after P563-PEtOx-*co*-PEI$_{30\%}$-*b*-PCL-DTX treatment, although the average reduction in tumor weight between the free DTX and P563-PEtOx-*co*-PEI$_{30\%}$-*b*-PCL-DTX groups was not statistically significant ($P=0.08$). These results suggest that DTX loaded into P563-PEtOx-*co*-PEI$_{30\%}$-*b*-PCL was slightly more efficient in decreasing tumor volume and weight when compared with free DTX.

All tumor types were characterized as Gleason score (GS) 5+5 prostate carcinoma in Histopathological analysis of the tumors, verifying that 22Rv1 prostate cancer xenograft mouse models were generated successfully. The average score of necrosis was 1 in the vehicle control and P563-PEtOx-*co*-PEI$_{30\%}$-*b*-PCL groups, 1.7 in the free DTX group (significantly higher compared with P563-PEtOx-*co*-PEI$_{30\%}$-*b*-PCL), and 1.2 in the P563-PEtOx-*co*-PEI$_{30\%}$-*b*-PCL-DTX group. The average score of inflammation was 1 in the vehicle control, P563-PEtOx-*co*-PEI$_{30\%}$-*b*-PCL, and free DTX groups and 0.6 in the P563-PEtOx-*co*-PEI$_{30\%}$-*b*-PCL-DTX group (statistically not significant compared with other groups). The average score of fibrosis was 1.3 in the vehicle control group, 1.7 in the P563-PEtOx-*co*-PEI$_{30\%}$-*b*-PCL and free DTX groups, and 1.2 in the P563-PEtOx-*co*-PEI$_{30\%}$-*b*-PCL-DTX group (significantly lower compared with P563-PEtOx-*co*-PEI$_{30\%}$-*b*-PCL and Free DTX groups) (Fig. 11, Table 2). Examination of the heart, liver, spleen, lung, and kidney tissue sections revealed no toxicity (Fig. 12).

Discussion

Prostate cancer is a major cause of death among men, and despite the relatively good response achieved by ADT, prevention of its recurrence relies on chemotherapeutic intervention, resulting in several adverse effects (Denmeade and Isaacs 2002). With the attempt to overcome this limitation, targeted therapy has become a research hot spot. Many studies have demonstrated improved efficacy and safety profiles for actively targeted drugs achieved by the conjugation of high-specificity tumor-homing peptides (Kondo et al. 2021). In prostate cancer, PSA and PSMA have emerged as the most effective targets, and high-affinity peptides that can specifically bind to these molecules have been identified by screening phage-display libraries (Shen et al. 2013). Previously, we have demonstrated that P563 was the most promising candidate among several peptides for active targeting of PSMA, with its ability to bind with high specificity to the cells showing even a moderate upregulation of this antigen (Nezir et al. 2021).

In light of these findings, our continued efforts have been focused on designing effective drug carriers specifically targeting PSMA. Polymeric micelles have been indicated as one of the most useful tools for drug delivery owing to the simplicity and versatility of their synthesis and functionalization (Mandracchia et al. 2014; Tripodo et al. 2013). PCL is a biodegradable polyester that has been in use for decades in the field of biomaterials and in tissue engineering as a drug delivery device (Woodruff and Hutmacher 2010; Kolluru 2020). PEtOx, a long-chain polymer with enhanced water solubility and biocompatibility, exerts low toxicity and no immunogenicity and is approved by FDA as a food additive (Adams and Schubert 2007; Zhang et al. 2020). Micelles composed of PEtOx polymers can resist protein adsorption and uptake by macrophages. Furthermore, the stability of the PEtOx main chain provides a chemical basis for further linking to targeting agents (Gao et al. 2019), making it a potential candidate to be used in targeted drug delivery. In this study, we investigated the efficacy of P563-PEtOx-*co*-PEI$_{30\%}$-*b*-PCL micelles in the delivery of DTX to PSMA-positive 22Rv1 prostate cancer cells.

In line with our previous study showing higher uptake of P563 by 22Rv1 prostate cancer cells, in vitro targeting experiments for P563- PEtOx-*co*-PEI$_{30\%}$-*b*-PCL polymeric micelles demonstrated a twofold higher affinity for cancer cells compared with normal prostate epithelial cells (Nezir et al. 2021). Next, we evaluated the effects of P563-PEtOx-*co*-PEI$_{30\%}$-*b*-PCL-DTX on cell viability. Although DTX in carriers and in free form had comparable effects at late time points, at 48 h, P563-PEtOx-*co*-PEI$_{30\%}$-*b*-PCL-DTX caused a significant 30% higher decrease in cancer cell viability, compared with the equal concentration of DTX in free form.

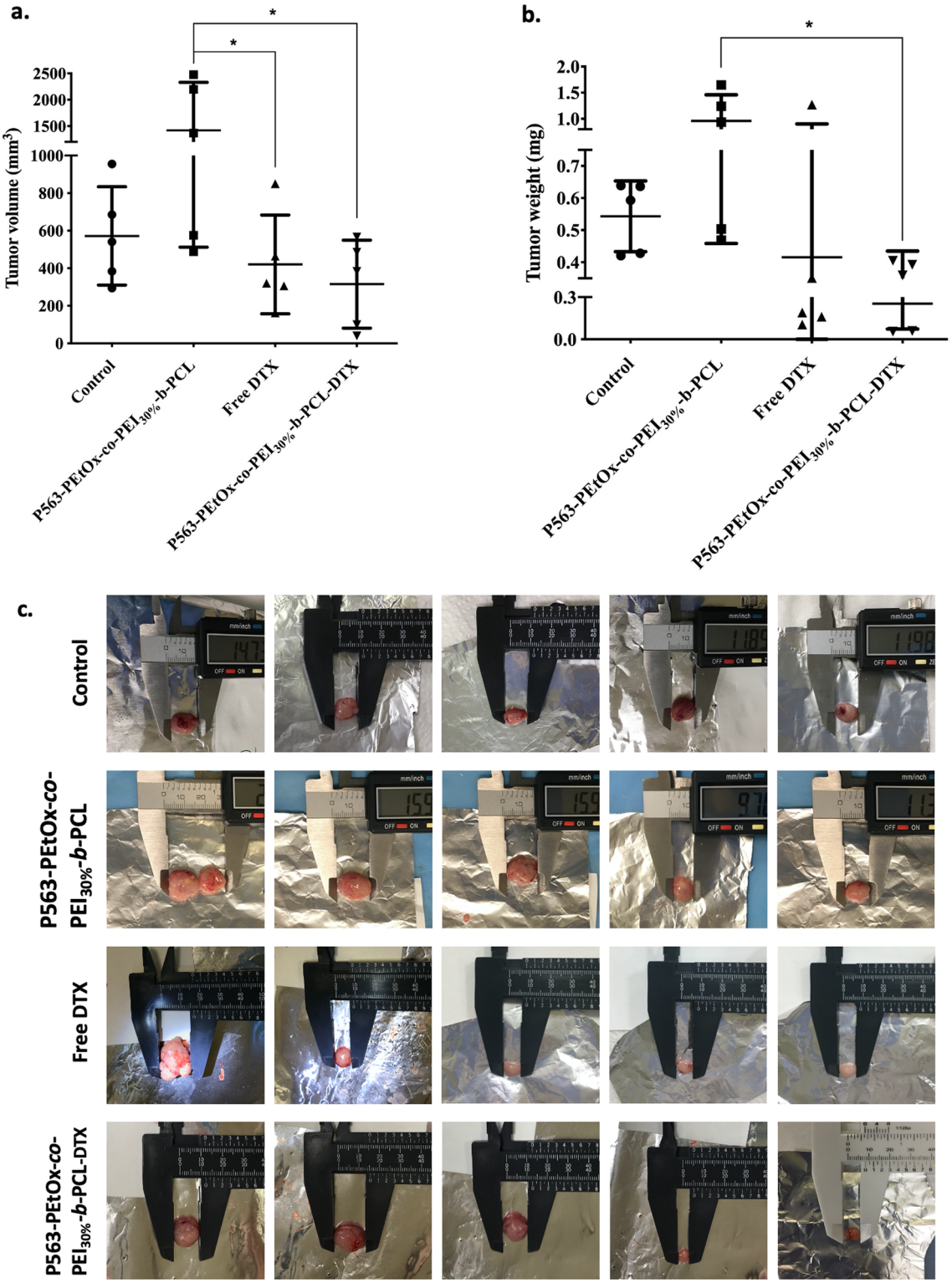

Fig. 10 Changes in **a** tumor volume and **b** tumor weight of CD-1 nu/nu male mice ($n=5$) upon treatment with the vehicle control, P563-PEtOx-*co*-PEI$_{30\%}$-*b*-PCL, free DTX, or P563-PEtOx-*co*-PEI$_{30\%}$-*b*-PCL-DTX. **c** Tumors collected from each animal ($n=5$). *$P \leq 0.05$, **$P \leq 0.01$

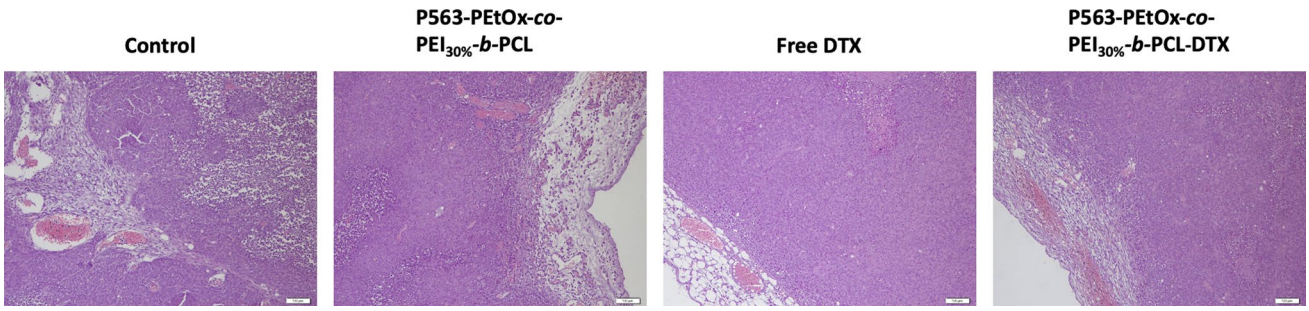

Fig. 11 Representative H&E staining images of the tumor tissue sections from the vehicle control, PEtOx-*co*-PEI$_{30\%}$-*b*-PCL, free DTX, and PEtOx-*co*-PEI$_{30\%}$-*b*-PCL-DTX groups. Scale bar: 100 µm

Table 2 Pathology scores of the experimental groups. 0, absent; 1, mild; 2, moderate; 3, severe

Group ($n=5$)	Necrosis	Inflammation	Fibrosis
Control	1	1	1.3
PEtOx-*co*-PEI$_{30\%}$-*b*-PCL	1	1	1.7
Free DTX	1.7*	1	1.7
PEtOx-*co*-PEI$_{30\%}$-*b*-PCL-DTX	1.2	0.6	1.2*$^{\#}$

*$P \leq 0.05$ (compared with PEtOx-*co*-PEI$_{30\%}$-*b*-PCL)

$^{\#}P \leq 0.05$ (compared with Free DTX)

This finding suggests that owing to active targeting, P563-PEtOx-*co*-PEI$_{30\%}$-*b*-PCL micelles could bind to PSMA and induce DTX internalization at an earlier time than free DTX that enters the cells through diffusion, resulting in faster cellular responses (Bhatia et al. 2018; Shen et al. 2013). This effect might also depend on the 200–400 nm size of the PEtOx-*co*-PEI$_{30\%}$-*b*-PCL NPs in the presence of serum, as 300-nm nanoparticles are known to be internalized with higher efficiency (Matsumura and Kataoka 2009).

The effect of P563-PEtOx-*co*-PEI$_{30\%}$-*b*-PCL-DTX on 22Rv1 prostate cancer cells depended in part on the induction of apoptosis, as demonstrated by the cleavage of caspases and PARP. Furthermore, although up to a 90% reduction in cell viability was observed upon treatment with P563-PEtOx-*co*-PEI$_{30\%}$-*b*-PCL-DTX, a 40% cell death was detected via the TUNEL assay. This difference between the percentages of cell death detected can be ascribed to the fact that the WST-1 assay shows the percentage of viable cells regardless of the mode of cell death, while TUNEL selectively discriminates the cells with DNA double-strand breaks (Kyrylkova et al. 2012).

For assessment of the in vivo efficacy of P563-PEtOx-*co*-PEI$_{30\%}$-*b*-PCL-DTX, xenograft models were established by subcutaneous injection of 22Rv1 cells into CD-1 nu/nu male mice, and drugs were administered i.p. every three days. In the literature, differing doses of DTX have been administered i.p. (2–60 mg/kg) or i.v. (12.5–13.4 mg/kg) for the evaluation of in vivo drug efficacy (Bourzat et al. 1995; van Beek et al. 2009; Hassan et al. 2011; Makhov et al. 2012; Jennings et al. 2002). We selected the lowest possible dose and administered 2 mg/kg/3d of DTX in our setting (a total dose of 16 mg/kg i.p.) to assess the cancer-specific targeting potential and efficacy of our drug-loaded formulation. The average body weight of mice did not change significantly during the 28 days of observation, suggesting a tolerable treatment dosage. Importantly, significant 57% and 74% reductions were noted in tumor volume after free DTX and P563-PEtOx-*co*-PEI$_{30\%}$-*b*-PCL-DTX administrations, respectively, compared with the empty carrier (P563-PEtOx-*co*-PEI$_{30\%}$-*b*-PCL). Consistently, DTX in the free form reduced the tumor weight by 78%, while P563-PEtOx-*co*-PEI$_{30\%}$-*b*-PCL-DTX administration resulted in a significant 84% reduction. These data imply that P563-PEtOx-*co*-PEI$_{30\%}$-*b*-PCL-DTX shows high tumor-regression activity against prostate cancer in vivo.

As demonstrated by both in vitro and in vivo assays, 0.1 mg/kg of PEtOx-*co*-PEI$_{30\%}$-*b*-PCL polymeric micelle used in our experiments induced the proliferation of normal prostate epithelial and prostate cancer cells. The respective 53% and 50% reductions in tumor volume and tumor weight relative to the control group (PBS) were observed for P563-PEtOx-*co*-PEI$_{30\%}$-*b*-PCL-DTX despite this stimulatory effect of the carrier itself on cell proliferation, indicating that, in fact, higher doses of DTX delivered by these NPs might exert a significant anticancer effect on prostate cancer cells, although this hypothesis remains to be tested in further studies.

An important indication of our study was the difference in histopathological findings between the treatment groups. Less necrotic tissue, inflammation, and fibrosis were observed in tissue biopsies of PEtOx-*co*-PEI$_{30\%}$-*b*-PCL-DTX-treated animals compared with those in the biopsies of the free DTX-treated group, implying that lower toxicity was exerted by an equal dose of the drug in the encapsulated form. These findings suggest that the side effects of DTX

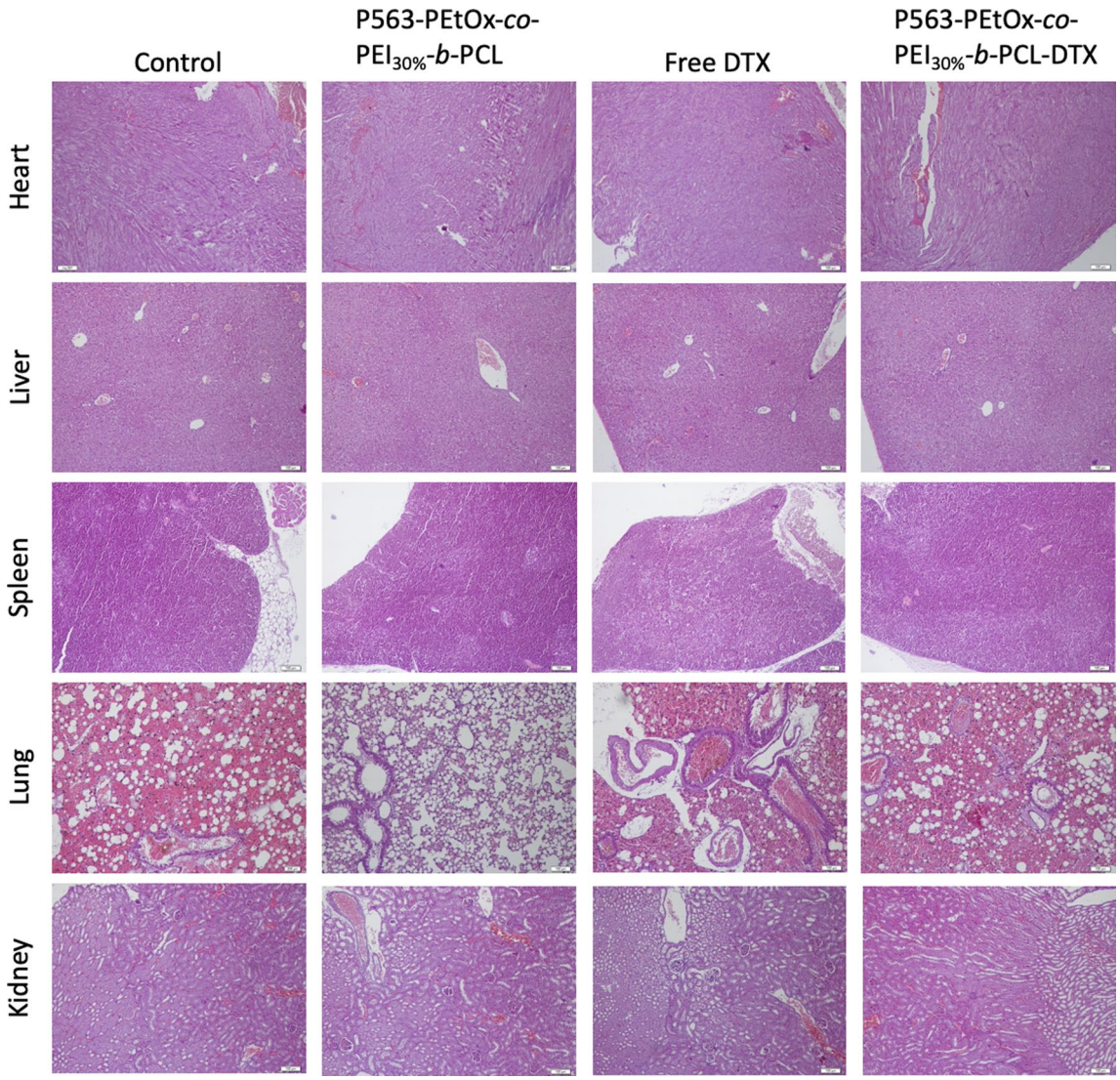

Fig. 12 Representative H&E staining images of the tissue sections from the vehicle control, PEtOx-*co*-$PEI_{30\%}$-*b*-PCL, free DTX, and PEtOx-*co*-$PEI_{30\%}$-*b*-PCL-DTX groups. Scale bar: 100 µm for the heart, liver, spleen, and kidney; 200 µm for the lung

may be reduced by encapsulation in PEtOx-*co*-$PEI_{30\%}$-*b*-PCL micelles.

In summary, this study showed for the first time that encapsulation of DTX in P563-conjugated PEtOx-*co*-$PEI_{30\%}$-*b*-PCL polymeric micelles has the potential to enhance the antitumor effect of the drug against prostate cancer. We have found that PEtOx-*co*-$PEI_{30\%}$-*b*-PCL-DTX NPs were efficiently taken up by prostate cancer cells, led to the inhibition of cancer cell proliferation, and displayed promising anti-cancer activity by inducing apoptosis. In vivo studies using 22Rv1 CD-1 nu/nu mouse models demonstrated that PEtOx-*co*-$PEI_{30\%}$-*b*-PCL-DTX showed a similar anti-cancer activity compared with free DTX but with lower toxicity, suggesting that better therapeutic outcomes can be expected through the targeted delivery of DTX at low doses with PEtOx-*co*-$PEI_{30\%}$-*b*-PCL polymeric micelles.

Acknowledgements Financial support from the Scientific and Technological Research Council of Turkey (TUBITAK, grant numbers 213M726 and 213M728) is gratefully acknowledged. All cell culture and animal experiments were conducted at Yeditepe University. We would like to thank Ayla Burcin Asutay and Murat Ozpolat for their technical support on flow cytometer. We also thank Engin Sumer, Ayse Hande Nayman, Halime Ilhan-Siginc, Selen Tiryaki, and Ipek Bedir for their technical support in the in vivo experiments.

Author contributions Conceptualization: AEN, NO, and DT; Development of methodology: AEN, NO, SG, UUO, IV, OY, AB, and DT; Investigation: AEN, ZBB, PK, IEZ and DT; Writing- Original Draft: AEN, NO, and DT; Writing-Review and Editing: DT and FS; Supervision: DT.

Data availability All data generated or analyzed during this study are included in this published article.

Declarations

Conflict of interest The authors declare no potential conflicts of interest.

References

Adams N, Schubert US (2007) Poly(2-oxazolines) in biological and biomedical application contexts. Adv Drug Deliv Rev 59:1504–1520. https://doi.org/10.1016/j.addr.2007.08.018

Alven S, Aderibigbe BA (2020) The therapeutic efficacy of dendrimer and micelle formulations for breast cancer treatment. Pharmaceutics 12:1212. https://doi.org/10.3390/pharmaceutics12121212

Barrio M, Fendler WP, Czernin J, Herrmann K (2016) Prostate specific membrane antigen (PSMA) ligands for diagnosis and therapy of prostate cancer. Expert Rev Mol Diagn 16:1177–1188. https://doi.org/10.1080/14737159.2016.1243057

Bhatia NM, Kulkarni PK, Ashtekar SS, Mahuli DV, Bhatia MS (2018) Synthesis, characterization, pharmacokinetics and evaluation of cytotoxicity for docetaxel-oleate conjugate targeting MCF-7 breast cancer cells. Pharm Chem J 51:1005–1013. https://doi.org/10.1007/s11094-018-1730-8

Bhattacharjee S (2016) DLS and zeta potential–what they are and what they are not? J of Control Release 235:337–351. https://doi.org/10.1016/j.jconrel.2016.06.017

Bill-Axelson A, Holmberg L, Ruutu M, Garmo H, Stark JR, Busch C, Nordling S, Häggman M, Andersson SO, Bratell S, Spångberg A, Palmgren J, Steineck G, Adami HO, Johansson JE, SPCG-4 Investigators (2011) Radical prostatectomy versus watchful waiting in early prostate cancer. N Engl J Med 364:1708–1717. https://doi.org/10.1056/NEJMoa1011967

Bourzat JD, Lavelle F, Commerçon A (1995) Synthesis and biological activity of Para-substituted 3′-phenyl docetaxel analogs. Bioorg Med Chem Lett 5:809–814. https://doi.org/10.1016/0960-894X(95)00118-D

Carter RE, Feldman AR, Coyle JT (1996) Prostate-specific membrane antigen is a hydrolase with substrate and pharmacologic characteristics of a neuropeptidase. Proc Natl Acad Sci USA 93:749–753. https://doi.org/10.1073/pnas.93.2.749

Chishti N, Jagwani S, Dhamecha D, Jalalpure S, Dehghan MH (2019) Preparation, optimization, and in vivo evaluation of nanoparticle-based formulation for pulmonary delivery of anticancer drug. Medicina (Kaunas) 55:294. https://doi.org/10.3390/medicina55060294

da Silva GH, Fernandes MA, Trevizan LNF, de Lima FT, Eloy JO, Chorilli MA (2018) Critical review of properties and analytical methods for the determination of docetaxel in biological and pharmaceutical matrices. Crit Rev Anal Chem 48:517–527. https://doi.org/10.1080/10408347.2018.1456315

Danaei M, Dehghankhold M, Ataei S, Hasanzadeh Davarani F, Javanmard R, Dokhani A, Khorasani S, Mozafari MR (2018) Impact of particle size and polydispersity index on the clinical applications of lipidic nanocarrier systems. Pharmaceutics 10:57. https://doi.org/10.3390/pharmaceutics10020057

Denmeade SR, Isaacs JT (2002) A history of prostate cancer treatment. Nat Rev Cancer 2:389–396. https://doi.org/10.1038/nrc801

Gao Y, Li Y, Li Y, Yuan L, Zhou Y, Li J, Zhao L, Zhang C, Li X, Liu Y (2015) PSMA-mediated endosome escape-accelerating polymeric micelles for targeted therapy of prostate cancer and the real time tracing of their intracellular trafficking. Nanoscale 7:597–612. https://doi.org/10.1039/c4nr05738d

Gao N, Xing C, Wang H, Feng L, Zeng X, Mei L (2019) pH-responsive dual drug-loaded nanocarriers based on poly (2-Ethyl-2-Oxazoline) modified black phosphorus nanosheets for cancer chemo/photothermal therapy. Front Pharmacol 10:270. https://doi.org/10.3389/fphar.2019.00270

Gulyuz S, Ozkose UU, Kocak P, Telci D, Yilmaz O, Tasdelen MA (2018) In-vitro cytotoxic activities of poly(2-ethyl-2-oxazoline)-based amphiphilic block copolymers prepared by CuAAC click chemistry. Express Polym Lett 12:146–158. https://doi.org/10.3144/expresspolymlett.2018.13

Gulyuz S, Ozkose UU, Khalily MP, Kesici MS, Kocak P, Bolat ZB, Kara A, Ozturk N, Ozcubukcu S, Bozkir A, Alpturk O, Telci D, Sahin F, Vural I, Yilmaz O (2021) Poly (2-ethyl-2-oxazoline-co-ethyleneimine)-block-poly (ε-caprolactone) based micelles: synthesis, characterization, peptide conjugation and cytotoxic activity. New J Chem 45:14532–14547. https://doi.org/10.1039/D1NJ01647D

Haberkorn U, Eder M, Kopka K, Babich JW, Eisenhut M (2016) New strategies in prostate cancer: prostate-specific membrane antigen (PSMA) ligands for diagnosis and therapy. Clin Cancer Res 22:9–15. https://doi.org/10.1158/1078-0432.CCR-15-0820

Hassan S, Buchanan M, Jahan K, Aguilar-Mahecha A, Gaboury L, Muller WJ, Alsawafi Y, Mourskaia AA, Siegel PM, Salvucci O, Basik M (2011) CXCR4 peptide antagonist inhibits primary breast tumor growth, metastasis and enhances the efficacy of anti-VEGF treatment or docetaxel in a transgenic mouse model. Int J Cancer 2:225–232. https://doi.org/10.1002/ijc.25665

Huggins C (1942) Effect of orchiectomy and irradiation on cancer. Ann Surg 115:1192–1200. https://doi.org/10.1097/00000658-194206000-00030

Imran M, Saleem S, Chaudhuri A, Ali J, Baboota S (2020) Docetaxel: an update on its molecular mechanisms, therapeutic trajectory and nanotechnology in the treatment of breast, lung and prostate cancer. J Drug Deliv Sci Tec 60:101959. https://doi.org/10.1016/j.jddst.2020.101959

Jennings D, Hatton BN, Guo J, Philippe J, Trouard TP, Raghunand N, Marshall J, Gillies RJ (2002) Early response of prostate carcinoma xenografts to docetaxel chemotherapy monitored with diffusion MRI. Neoplasia 4:255–262. https://doi.org/10.1038/sj.neo.7900225

Kara A, Ozturk N, Esendagli G, Ozkose UU, Gulyuz S, Yilmaz O, Telci D, Bozkir A, Vural I (2018) Development of novel self-assembled polymeric micelles from partially hydrolysed poly(2-ethyl-2-oxazoline)-co-PEI-b-PCL block copolymer as non-viral vectors for plasmid DNA in vitro transfection. Artif Cell Nanomed B 46:S264–S273. https://doi.org/10.1080/21691401.2018.1491478

Kiess AP, Banerjee SR, Mease RC, Rowe SP, Rao A, Foss CA, Chen Y, Yang X, Cho SY, Nimmagadda S, Pomper MG (2015) Prostate-specific membrane antigen as a target for cancer imaging and therapy. Q J Nucl Med Mol Imaging 59:241–268 (**PMID: 26213140**)

Kolluru LP, Chandran T, Shastri PN, Rizvi SAA, D'Souza MJ (2020) Development and evaluation of polycaprolactone based docetaxel nanoparticle formulation for targeted breast cancer therapy. J Nanopart Res 22:372. https://doi.org/10.1007/s11051-020-05096-y

Kondo E, Iioka H, Saito K (2021) Tumor-homing peptide and its utility for advanced cancer medicine. Cancer Sci 112:2118–2125. https://doi.org/10.1111/cas.14909

Kyrylkova K, Kyryachenko S, Leid M, Kioussi C (2012) Detection of apoptosis by TUNEL assay. Methods Mol Biol 887:41–47. https://doi.org/10.1007/978-1-61779-860-3

Litwin MS, Tan HJ (2017) The diagnosis and treatment of prostate cancer: a review. JAMA 317:2532–2542. https://doi.org/10.1001/jama.2017.7248

Mahmood MA, Madni A, Rehman M, Rahim MA, Jabar A (2019) Ionically cross-linked chitosan nanoparticles for sustained delivery of docetaxel: fabrication, post-formulation and acute oral toxicity evaluation. Int J Nanomedicine 14:10035–10046. https://doi.org/10.2147/IJN.S232350

Makhov P, Golovine K, Canter D, Kutikov A, Simhan J, Uzzo CMM, RG, Kolenko VM, (2012) Co-administration of piperine and docetaxel results in improved anti-tumor efficacy via inhibition of CYP3A4 activity. Prostate 72:661–667. https://doi.org/10.1002/pros.21469

Mandracchia D, Tripodo G, Latrofa A, Dorati R (2014) Amphiphilic inulin-d-α-tocopherol succinate (INVITE) bioconjugates for biomedical applications. Carbohydr Polym 103:46–54. https://doi.org/10.1016/j.carbpol.2013.11.056

Matsumura Y, Kataoka K (2009) Preclinical and clinical studies of anticancer agent-incorporating polymer micelles. Cancer Sci 100:572–579. https://doi.org/10.1111/j.1349-7006.2009.01103.x

Mudalige T, Qu H, Van Haute D, Ansar SM, Paredes A, Ingle T (2019) Characterization of nanomaterials: tools and challenges. In: López Rubio A (ed) Nanomaterials for food applications. Elsevier, pp 313–353. https://doi.org/10.1016/B978-0-12-814130-4.00011-7

Narvekar M, Xue HY, Eoh JY, Wong HL (2014) Nanocarrier for poorly water-soluble anticancer drugs—barriers of translation and solutions. AAPS PharmSciTech 15:822–833. https://doi.org/10.1208/s12249-014-0107-x

Nayman AH, Siginc H, Zemheri E, Yencilek F, Yildirim A, Telci D (2019) Dual-inhibition of mTOR and Bcl-2 enhances the antitumor effect of everolimus against renal cell carcinoma in vitro and in vivo. J Cancer 10:1466–1478. https://doi.org/10.7150/jca.29192

Nezir AE, Khalily MP, Gulyuz S, Ozcubukcu S, Kucukguzel SG, Yilmaz O, Telci D (2021) Synthesis and evaluation of tumor-homing peptides for targeting prostate cancer. Amino Acids 53:645–652. https://doi.org/10.1007/s00726-021-02971-3

Ozturk N, Kara A, Gulyuz S, Ozkose UU, Tasdelen MA, Bozkir A, Yilmaz O, Vural I (2020) Exploiting ionisable nature of PEtOx-co-PEI to prepare pH sensitive, doxorubicin-loaded micelles. J Microencapsul 37:467–480. https://doi.org/10.1080/02652048.2020.1792566

Salji MJ, Ahmad I, Slater S, Poon FW, Alhasso A, Melquiot NV, Bekarma H, Hendry J, Leung HY (2019) Prostate neoplasm. In: Aboumarzouk OM (ed) Blandy's urology, 3rd edn. Wiley, New York. https://doi.org/10.1002/9781118863343.ch28

Shen D, Xie F, Edwards WB (2013) Evaluation of phage display discovered peptides as ligands for prostate-specific membrane antigen (PSMA). PLoS One 8:1–8. https://doi.org/10.1371/journal.pone.0068339

Tan Q, Liu X, Fu X, Li Q, Dou J, Zhai G (2012) Current development in nanoformulations of docetaxel. Expert Opin Drug Deliv 9:975–990. https://doi.org/10.1517/17425247.2012.696606

Thambiraj S, Vijayalakshmi R, Shankaran DR (2021) An effective strategy for development of docetaxel encapsulated gold nanoformulations for treatment of prostate cancer. Sci Rep 11:2802. https://doi.org/10.1038/s41598-020-80529-1

Tripodo G, Mandracchia D, Dorati R, Latrofa A, Genta I, Conti B (2013) Nanostructured polymeric functional micelles for drug delivery applications. Macromole Symp 334:17–23. https://doi.org/10.1002/masy.201300099

Tripodo G, Mandracchia D, Collina S, Rui M, Rossi D (2014) New perspectives in cancer therapy: the biotin-antitumor molecule conjugates. Med Chem S1:1–8. https://doi.org/10.4172/2161-0444.S1-004

van Beek ER, Lowik CWGM, van Wijngaarden J, Ebetino FH, Papapoulos SE (2009) Synergistic effect of bisphosphonate and docetaxel on the growth of bone metastasis in an animal model of established metastatic bone disease. Breast Cancer Res Treat 118:307–313. https://doi.org/10.1007/s10549-008-0236-6

Varela-Moreira A, Shi Y, Fens MHAM, Lammers T, Hennink WE, Schiffelers RM (2017) Clinical application of polymeric micelles for the treatment of cancer. Mater Chem Front 1:1485–1501. https://doi.org/10.1039/C6QM00289G

Wang Y, Zuo A, Huang X, Ying Y, Shu X, Chen X, Yang Y, Ma J, Lin G, Wang X, Mei L, Liu G, Zhao Y (2019) Docetaxel-loaded PAMAM-based poly (γ-benzyl-l-glutamate)-b-d-α-tocopheryl polyethylene glycol 1000 succinate nanoparticles in human breast cancer and human cervical cancer therapy. J Microencapsul 36:552–565. https://doi.org/10.1080/02652048.2019.1654002

Woodruff MA, Hutmacher DW (2010) The return of a forgotten polymer—polycaprolactone in the 21st century. Prog Polym Sci. https://doi.org/10.1016/j.progpolymsci.2010.04.002

Wüstemann T, Haberkorn U, Babich J, Mier W (2018) Targeting prostate cancer: prostate-specific membrane antigen based diagnosis and therapy. Med Res Rev 39:40–69. https://doi.org/10.1002/med.21508

Yokoyama M (2014) Polymeric micelles as drug carriers: their lights and shadows. J Drug Target 22:576–583. https://doi.org/10.3109/1061186X.2014.934688

Zhang L, Zhang N (2013) How nanotechnology can enhance docetaxel therapy. Int J Nanomedicine 8:2927–2941. https://doi.org/10.2147/IJN.S46921

Zhang X, Liu J, Li X, Li F, Lee RJ, Sun F, Li Y, Liu Z, Teng L (2019) Trastuzumab-coated nanoparticles loaded with docetaxel for breast cancer therapy. Dose Response 17:1559325819872583. https://doi.org/10.1177/1559325819872583

Zhang H, Liu X, Xu T, Xu K, Du B, Li Y (2020) Biodegradable reduction and pH dual-sensitive polymer micelles based on poly (2-ethyl-2-oxazoline) for efficient delivery of curcumin. RSC Adv 10:25435–25445. https://doi.org/10.1039/D0RA02779K

Zhao Y, Dandan S, Shang M, Sun X, Guo L, Meng D, Liu X, Zhou X, Li J (2022) GRP78-targeted and doxorubicin-loaded nanodroplets combined with ultrasound: a potential novel theranostics for castration-resistant prostate cancer. Drug Delivery 29:203–213. https://doi.org/10.1080/10717544.2021.2023698